Use of high-resolution geophysical data to characterize heterogeneous aquifers: Influence of data integration method on hydrological predictions

B. Dafflon,[1] J. Irving,[1] and K. Holliger[1]

Received 10 December 2008; revised 19 May 2009; accepted 11 June 2009; published 11 September 2009.

[1] The integration of geophysical data into the subsurface characterization problem has been shown in many cases to significantly improve hydrological knowledge by providing information at spatial scales and locations that is unattainable using conventional hydrological measurement techniques. The investigation of exactly how much benefit can be brought by geophysical data in terms of its effect on hydrological predictions, however, has received considerably less attention in the literature. Here, we examine the potential hydrological benefits brought by a recently introduced simulated annealing (SA) conditional stochastic simulation method designed for the assimilation of diverse hydrogeophysical data sets. We consider the specific case of integrating crosshole ground-penetrating radar (GPR) and borehole porosity log data to characterize the porosity distribution in saturated heterogeneous aquifers. In many cases, porosity is linked to hydraulic conductivity and thus to flow and transport behavior. To perform our evaluation, we first generate a number of synthetic porosity fields exhibiting varying degrees of spatial continuity and structural complexity. Next, we simulate the collection of crosshole GPR data between several boreholes in these fields, and the collection of porosity log data at the borehole locations. The inverted GPR data, together with the porosity logs, are then used to reconstruct the porosity field using the SA-based method, along with a number of other more elementary approaches. Assuming that the grid-cell-scale relationship between porosity and hydraulic conductivity is unique and known, the porosity realizations are then used in groundwater flow and contaminant transport simulations to assess the benefits and limitations of the different approaches.

Citation: Dafflon, B., J. Irving, and K. Holliger (2009), Use of high-resolution geophysical data to characterize heterogeneous aquifers: Influence of data integration method on hydrological predictions, *Water Resour. Res.*, *45*, W09407, doi:10.1029/2008WR007646.

1. Introduction

[2] It is well established that knowledge regarding spatial heterogeneity in hydrological properties is required for effective modeling of subsurface contaminant transport [e.g., *Gelhar*, 1993; *Hubbard and Rubin*, 2005; *Sudicky and Huyakorn*, 1991; *Zheng and Gorelick*, 2003]. To this end, high-resolution geophysical methods have shown much potential to bridge a gap in terms of resolution and subsurface coverage between traditional hydrological measurement techniques such as borehole log/core analyses and tracer/well tests [e.g., *Hubbard et al.*, 2001; *Hyndman and Gorelick*, 1996]. Whereas geophysical data were initially used in hydrology to qualitatively delineate the general architecture of the subsurface [e.g., *Asprion and Aigner*, 1999; *Beres et al.*, 1995; *Bowling et al.*, 2005], recent efforts have focused on the determination of detailed quantitative information from these data [e.g., *Chen et al.*, 2001; *Harp et al.*, 2008; *Hyndman et al.*, 2000; *Kowalsky et al.*, 2005; *Linde et al.*, 2006; *Paasche et al.*, 2006]. The general idea behind this work is that, when combined with other site measurements, high-resolution geophysical data can be used to significantly improve our knowledge regarding the spatial distribution of subsurface hydrological parameters. This knowledge can then be used to improve models and thus predictions of flow and transport [e.g., *Hubbard et al.*, 2001; *Hyndman and Gorelick*, 1996; *McKenna and Poeter*, 1995; *Scheibe and Chien*, 2003].

[3] One class of methods for the reconstruction of hydrological property fields using geophysical and other data is conditional stochastic simulation [e.g., *Hyndman et al.*, 2000; *McKenna and Poeter*, 1995; *Tronicke and Holliger*, 2005]. With this class of methods, multiple configurations of subsurface properties are generated that are consistent with all available data, constraints, and prior information. In general, the data can be characterized by various degrees of resolution and/or hardness and the constraints may be deterministic and/or stochastic in nature. All of the resulting property distributions are then considered as possible based on the available information. In other words, the variability between the generated realizations tends to describe our uncertainty regarding the true hydrological property field. This uncertainty in turn can be used to evaluate our

[1] Institute of Geophysics, University of Lausanne, Lausanne, Switzerland.

0043-1397/09/2008WR007646$09.00

uncertainty regarding groundwater flow and contaminant transport. All of this is important because it is well known that single "best" estimates of subsurface properties tend to be too smooth for reliable hydrological predictions [e.g., *Robinson et al.*, 2008; *Scheibe and Chien*, 2003].

[4] One type of conditional simulation technique that has shown much promise for the integration of complex data sets in both petroleum and hydrological studies is simulated annealing (SA) [e.g., *Dafflon et al.*, 2009; *Day-Lewis et al.*, 2000; *Deutsch and Cockerham*, 1994; *Deutsch and Journel*, 1998; *Deutsch and Wen*, 1998; *Kelkar and Perez*, 2002; *Parks et al.*, 2000; *Tronicke and Holliger*, 2005]. With the SA method, a Monte-Carlo approach is used to successively perturb an initial starting realization in order to satisfy the structural and/or petrophysical constraints imposed by the available data. This is done through a multiobjective optimization process. Recently, *Dafflon et al.* [2009] introduced a novel SA-based conditional simulation approach for the assimilation of hydrogeophysical data sets having varying degrees of resolution, subsurface coverage, and sensitivity to the parameter of interest. In testing this approach on synthetic data composed of crosshole GPR tomograms and borehole porosity logs, they were able to generate realizations of porosity having an unprecedented degree of realism when compared to the true subsurface porosity structure. The approach was also tested with much success on field crosshole GPR and neutron porosity log data from the Boise Hydrogeophysical Research Site, Idaho, USA. However, one issue that is as-of-yet unexplored with this technique involves its potential hydrological benefits in terms of groundwater flow and contaminant transport predictions. Hydrological evaluation of the obtained realizations is critical to understanding the potential value of such an integration procedure, and indeed the value of high-resolution geophysical data in general, in hydrological studies.

[5] In the above context, one study of particular interest is that of *Scheibe and Chien* [2003], who evaluated the impact of integrating various amounts of geophysical and hydrological data on tracer transport predictions at a field site near Oyster, Virginia. In the study, several procedures to infer the subsurface hydraulic conductivity distribution were examined, including the simple use of a homogeneous model obtained from the average of borehole flowmeter measurements, the use of sequential indicator simulation conditioned to these flowmeter measurements, and the use of sequential indicator simulation conditioned to both geophysical tomograms and the flowmeter data. In this last case, hydraulic conductivity data between the boreholes, which were estimated from the tomograms using a normal linear regression model based on collocated data at the borehole locations, were considered as hard data in the simulation process. The results of *Scheibe and Chien* [2003] showed that conditioning to data with larger spatial support scales (i.e., the cross-sectional estimates of hydraulic conductivity based on geophysical tomography) provided a significant improvement in hydrological model accuracy.

[6] In this paper, we work along the same lines as *Scheibe and Chien* [2003] in order to evaluate the potential hydrological benefits of tomographic geophysical data and the implications of using various integration techniques on the output hydrological predictions. In particular, we attempt to assess hydrologically the SA-based method of *Dafflon et al.* [2009], in comparison with other more basic approaches, in the context of porosity characterization in heterogeneous aquifers using crosshole GPR and porosity log data. In contrast to *Scheibe and Chien* [2003], we do this for three different synthetic models possessing various degrees of structural complexity, such that the advantages and disadvantages between the methods under different structural conditions can be examined. It is important to note that we consider a best case scenario for this work, which involves assuming a unique and known small-scale relationship between porosity and hydraulic conductivity for the hydrological evaluation, optimal measurement conditions, and some knowledge regarding the geostatistical structure of the subsurface. Although admittedly such strong assumptions limit the direct applicability of our results to a field setting, they allow us to effectively evaluate the greatest potential benefits of each method in terms of its ability to capture realistic subsurface structure, and how this translates into an ability to perform accurate flow and transport simulations.

[7] The paper proceeds as follows. First, we briefly outline the SA approach to data integration, as well as the pertinent features of the new algorithm presented by *Dafflon et al.* [2009]. Next, we describe the process via which we assess hydrologically the potential benefits of this and the other more basic characterization methods. This involves (1) generating a set of realistic subsurface models exhibiting varying degrees of lateral continuity and structural complexity, (2) numerically modeling the corresponding geophysical data, (3) integrating these data to obtain the subsurface porosity distribution using the SA method and other techniques, and (4) converting porosity to hydraulic conductivity and performing flow and transport simulations. Finally, we examine the results obtained for our suite of models in terms of how well each technique allows for successful hydrological predictions.

2. SA-Based Conditional Simulation

[8] Simulated annealing is a directional Monte-Carlo-type optimization method that involves repeatedly perturbing values of a target parameter field in order to satisfy a global objective function. This function generally consists of a weighted sum of several component objective functions, each representing a different constraint on the output realizations [e.g., *Deutsch and Journel*, 1998]. All perturbations that lower the global objective function are unconditionally accepted, whereas those that do not are accepted according to a Boltzmann-type probability distribution controlled by a temperature parameter T. The higher the value of T, the more likely an unfavorable perturbation will be accepted. Throughout the SA process, T is lowered gradually such that the algorithm has a chance to reach an optimal "energy state". Once the global objective function is deemed small enough, the SA procedure is terminated. Advantages of using the SA approach for data integration are that it is not limited to simple Gaussian statistics, and it is able to incorporate any constraint on the output realizations that can be expressed in the form of a multicomponent objective function. This of course comes with the caveat that efficiency in terms of computation time and convergence decreases with constraint complexity. For further information on the use of SA for subsurface data integra-

tion, we refer the reader to the works of *Deutsch and Cockerham* [1994], *Deutsch and Journel* [1998], *Deutsch and Wen* [1998], *Day-Lewis et al.* [2000], *Parks et al.* [2000], *Kelkar and Perez* [2002], *Tronicke and Holliger* [2005], and *Dafflon et al.* [2009].

[9] Recently *Dafflon et al.* [2009] presented a novel SA algorithm for the integration of high-resolution geophysical and hydrological data. In comparison with more conventional SA-based integration approaches [e.g., *Tronicke and Holliger*, 2005], this method provides significant advancements in the way that large-scale structural information in the geophysical data is accounted for, which results in a substantial improvement in the parameter fields obtained. One major novelty in the approach of *Dafflon et al.* [2009] is that model perturbations in the SA procedure are made by drawing from a conditional probability distribution for the target parameter, given the available tomographic geophysical data. This is the only place where geophysical information is utilized in the algorithm, which is in marked contrast to previous approaches where model perturbations were made through the swapping of values in the simulation grid and agreement with the geophysical data was enforced through a correlation coefficient constraint. Another major feature of the algorithm concerns the target variogram function and the way in which available geostatistical information is utilized. Instead of constraining output realizations to match a parametric target variogram model over a wide range of spatial lags, realizations are constrained only at smaller lags where the geophysical data cannot provide enough information. Thus the larger-scale subsurface features, which are well constrained by the geophysical data, are allowed much more control on the output realizations.

[10] As mentioned previously, *Dafflon et al.* [2009] applied their SA-based method to crosshole GPR and porosity log data in order to characterize the porosity distribution in saturated heterogeneous aquifers. In tests on both synthetic and field data, this algorithm showed much greater capacity than other more conventional approaches to incorporate the larger-scale subsurface structure provided by the geophysical data, while at the same time realistically introducing smaller-scale stochastic fluctuations from the utilized parametric variogram model. An additional advantage of this method is that, because of a dramatically simplified global objective function, the algorithm exhibits very favourable characteristics with regard to convergence and computational efficiency, and has less subjectivity associated with choosing the weighting of many objective function components.

[11] In this study, we use the algorithm of *Dafflon et al.* [2009] to generate realizations of the subsurface porosity field given crosshole GPR and porosity log data with the objective of evaluating these realizations in a hydrological context. As mentioned, we do this under a best-case scenario, where one of our key assumptions is complete knowledge of the relationship between porosity and hydraulic conductivity. To obtain the conditional probability distribution for porosity given the available geophysical data, which is required to perform the model perturbations with the method of *Dafflon et al.* [2009], we follow their paper and use a simple parametric approach based on the analysis of collocated data at the borehole locations. From a scatter plot of the collocated GPR velocity and borehole porosity logs, we estimate the conditional expectation $E(\phi|v)$ and the corresponding conditional variance $\sigma^2(\phi|v)$, where ϕ denotes porosity and v the GPR velocity. We assume that the expectation follows a linear relationship and that the variance is constant, and that these are sufficient to define the conditional distribution. This distribution is used at every subsurface location except at the boreholes, where it is more tightly constrained by the porosity log data. Although we are aware that the velocity-porosity relationship can vary with location in the tomogram because of differences in resolution throughout the image plane [e.g., *Day-Lewis and Lane*, 2004], we feel that this approach is pragmatic since the conditional distribution we infer is worst at the borehole locations, which means that the generated realizations will be under- rather than overconstrained by the tomographic data. Also note that other methods could be used to infer such a conditional distribution, such as for example the Bayesian approach presented by *Chen et al.* [2001]. In that work, a normal linear regression model was used to explore the relationship between collocated tomographic GPR velocity and borehole hydraulic conductivity data. This relationship was then used to update a prior probability density function (pdf) for the hydraulic conductivity field, obtained by kriging the borehole measurements, into a posterior pdf taking into account the GPR data.

[12] Also required in the algorithm of *Dafflon et al.* [2009] is a variogram function to constrain the small-scale structure of the target parameter field. In other words, at scales where the subsurface structure is not well resolved by the geophysical data, it is constrained stochastically. To obtain this target variogram function, we calculate the best fitting parametric model to the vertical experimental variogram of the porosity logs at short lags, and we assume a known aspect ratio between the horizontal and vertical directions. This assumption is justified by the fact that, with our SA approach, the effect of the aspect ratio is quite limited because the target variogram affects principally the small-scale structure. This is clearly seen in the Figure 5 of *Dafflon et al.* [2009]. Large-scale structure, in contrast, is provided by the geophysical image through the use of the above described conditional probability distributions. Further, it may be possible to use the tomographic image to estimate the variogram aspect ratio assuming that this ratio remains constant across scales. To choose the variogram cutoff lag for the SA procedure (i.e., the lag beyond which we do not constrain the output realizations to the target variogram model), we consider the estimated resolution of the geophysical image. We set the cutoff to be larger in the horizontal direction because of the restricted horizontal resolution of crosshole tomographic data as a result of survey geometry. For more details on this procedure, please see the work of *Dafflon et al.* [2009].

3. Hydrological Evaluation Procedure

[13] The principal aim of this study is to investigate the potential hydrological benefits brought by using the above SA approach to data integration, in comparison with other more basic characterization strategies, under the most optimal conditions. To do this, we consider three realistic, synthetic, 2-D porosity fields exhibiting varying degrees

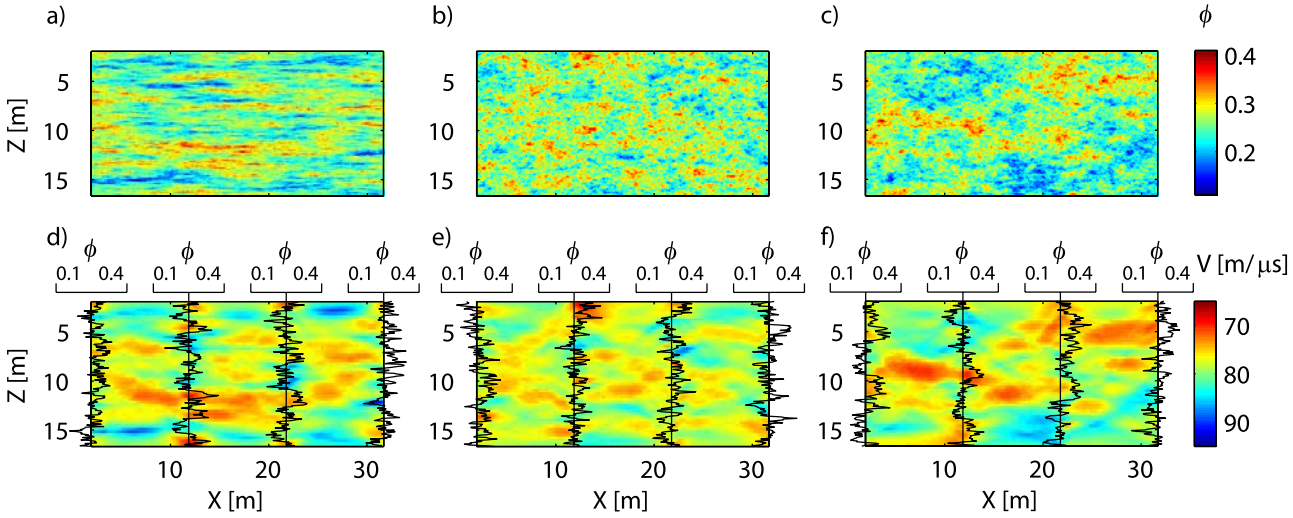

Figure 1. Original ("true") porosity model having (a) large horizontal-to-vertical aspect ratio and relatively small vertical correlation length (Example 1), (b) small horizontal-to-vertical aspect ratio and relatively small vertical correlation length (Example 2), and (c) small horizontal-to-vertical aspect ratio and relatively large vertical correlation length (Example 3). (d–f) Result of traveltime inversion of the three synthetic, crosshole georadar data sets simulated between boreholes located at 0, 10, 20, and 30 m lateral distance from the left model edge and the simulated borehole porosity logs. See also Table 1.

of lateral continuity and structural complexity. With these fields, crosshole GPR and borehole porosity log data are simulated. The GPR and porosity log data are then used in the SA and other procedures to reconstruct the subsurface porosity distribution. Finally, to assess the hydrological significance of the results, we assume a unique and known relationship between porosity and hydraulic conductivity and conduct groundwater flow and solute transport simulations. It is very important to emphasize that assuming a porosity-hydraulic conductivity relationship in this manner is a big step, and not valid in many field scenarios. However, in terms of our objectives, we feel that the assumption is appropriate in that it allows us to examine the potential hydrological benefits of reintroducing small-scale heterogeneity, as well as the effects of possible biases that occur when reconstructing the hydrological property distribution. In addition, although the hydraulic conductivity depends on a number of parameters other than porosity [e.g., *Freeze and Cherry*, 1979; *Schön*, 2004], a strong relationship may exist between these two parameters in sand and/or gravel-type materials [e.g., *Hubbard et al.*, 1999]. Such electrically resistive materials in turn are required for effective GPR imaging. Indeed, GPR has allowed the successful estimation of hydraulic conductivity in a number of such environments [e.g., *Chen et al.*, 2001; *Hubbard et al.*, 1999; *Scheibe and Chien*, 2003]. In the following section, we describe each of the steps involved in our hydrological evaluation procedure in detail.

3.1. Hydrological Property Models

[14] Three realistic stochastic porosity fields exhibiting varying degrees of lateral continuity and structural complexity were generated. The statistical characteristics of these fields, which we refer to as Examples 1, 2, and 3, are described in Table 1. The porosity field in Example 1 (Figure 1a) has a horizontal-to-vertical aspect ratio of 10 and its horizontal variogram is well fitted by a linear combination of two exponential functions having sills of 0.45 and 0.55 and ranges of 3 m and 15 m, respectively. This field is representative of scenarios where large lateral continuity and relatively thin layers are present. The porosity field in Example 2 (Figure 1b) has an aspect ratio of 2 and its horizontal variogram is well fitted by two exponential functions having sills of 0.5 and 0.5 and ranges of 0.6 m and 4 m. This field represents situations where we have little horizontal and vertical continuity, and a small amount of structural anisotropy. Finally, the porosity field in Example 3 (Figure 1c) has an aspect ratio of 2.5 and a horizontal variogram that is well fitted by functions having sills of 0.55 and 0.45 and ranges of 1.5 m and 11.25 m. This field is representative of scenarios where we have a small amount of structural anisotropy, but relatively large horizontal and vertical continuity.

[15] All of the porosity models described in Table 1 and shown in Figures 1a–1c have a mean porosity value of 0.26 and a standard deviation of 0.035. This can be regarded as typical of unconsolidated clastic sediments consisting predominantly of sand and gravel [e.g., *Gelhar*, 1993; *Heinz et al.*, 2003]. The models are discretized at 7.5 cm increments in the x and z directions, and boreholes are considered at lateral positions of 0, 10, 20, and 30 m from the left model edge. Another key feature of all of the models is that they visibly exhibit heterogeneity at a range of spatial scales. They can thus be regarded as challenging and pertinent test cases.

[16] For all of our examples, we assume a known unique linear relationship between porosity and the logarithm of hydraulic conductivity (K) at the scale of a grid cell (7.5 cm). This relationship is of the form $\log_{10}(K) = 6.66\ \phi - 4.97$, which yields hydraulic conductivities within an interval that is typical for sand and gravel [e.g., *Gelhar*, 1993; *Heinz et al.*, 2003; *Hubbard et al.*, 2001; *Schön*, 2004]. The goal is then to evaluate flow and transport through these models and compare this "true" behavior with that predicted

Table 1. Characteristics of the Three Synthetic Porosity Models and the Assigned Relationships to Hydraulic Conductivity[a]

	Example 1	Example 2	Example 3
Description	Large aspect ratio, small vertical correlation length	Small aspect ratio, small vertical correlation length	Small aspect ratio, large vertical correlation length
Aspect ratio (a_x/a_z)	10	2	2.5
Experimental variogram function type	Exponential	Exponential	Exponential
[*Sill1* a_{z1} a_{x1}]	[0.45 0.3 3]	[0.5 0.3 0.6]	[0.55 0.6 1.5]
[*Sill2* a_{z2} a_{x2}]	[0.55 1.5 15]	[0.5 2 4]	[0.45 4.5 11.25]
Mean of ϕ	0.2587	0.2603	0.2590
Standard deviation of ϕ	0.0357	0.0343	0.0347
Slope of $\log_{10}(K)$ vs. ϕ	6.6667	6.6667	6.6667
Intercept at $\phi = 0$	−4.9677	−4.9677	−4.9677
Mean of $\log_{10}(K)$	−3.2433	−3.2325	−3.2411
Standard deviation of $\log_{10}(K)$	0.2377	0.2286	0.2315
Relationship inferred from collocated data:	$a = -5.54 \times 10^{-3}$	$a = -5.23 \times 10^{-3}$	$a = -7.67 \times 10^{-3}$
$E(\phi\|v) = av + b$	$b = 0.694$	$b = 0.672$	$b = 0.862$
$\sigma(\phi\|v)$	0.030	0.032	0.029

[a]The experimental variogram function of the models is best fitted by the sum of two exponentials having variances (*Sill1*, *Sill2*) and ranges (a_{x1}, a_{x2}, a_{z1}, a_{z2}). The range is defined as the lag distance where the variogram function reaches 95% of the sill value. To infer the hydraulic conductivity from porosity, we assume a linear relationship between ϕ and $\log_{10}(K)$.

using the porosity reconstructions obtained from the different methods.

3.2. Geophysical Measurements

[17] From the porosity models shown in Figures 1a–1c, synthetic borehole porosity logs and crosshole GPR data were simulated. For the porosity log data, vertical traces were extracted from the model at the defined borehole locations (Figures 1d–1f). Consequently, the log data in this study are simply unbiased in-situ measurements of the actual porosity at the borehole locations with a resolution on the order of a grid cell (7.5 cm). Although this is clearly a simplification of real porosity log data, which will contain a small amount of smoothing related to the support volume of the measurement, we feel that it is an adequate approximation for our purposes. Further, biases in the porosity-log measurements would influence the results of all of the tested characterization approaches and thus not change drastically the conclusions obtained.

[18] To create the crosshole GPR data, three tomography surveys were simulated between all adjacent pairs of wells in the synthetic models. As a first step, the porosity models in Figures 1a–1c needed to be converted to subsurface electrical properties. To obtain values for the relative dielectric permittivity, the complex refractive index model (CRIM) equation for saturated media was used [e.g., *Schön*, 2004]:

$$\sqrt{\varepsilon_r} = \phi\sqrt{\varepsilon_r^w} + (1-\phi)\sqrt{\varepsilon_r^m}, \quad (1)$$

where ε_r^m and $\varepsilon_r^w = 80$ are the relative dielectric permittivities of the dry matrix and water, respectively. For this study, a value of $\varepsilon_r^m = 4.6$ was employed, which is typical for unconsolidated sand and gravel sediments [e.g., *Schön*, 2004]. For the electrical conductivity of the subsurface region, a constant value of 1 mS/m was assumed. Finally, because surficial soils and rocks are generally nonmagnetic, we assumed that the magnetic permeability is equal to its free-space value throughout the simulation region [e.g., *Davis and Annan*, 1989].

[19] Using the above electrical properties, full-waveform GPR data were computed using a finite-difference time-domain (FDTD) solution of Maxwell's equations in 2-D cylindrical coordinates [*Holliger and Bergmann*, 2002]. This efficient and accurate computational method predicts all direct, refracted, reflected, and scattered electromagnetic waves and accounts for the inherent 3-D radiation and geometric spreading characteristics of dipole transmitters and receivers. The transmitter antenna was approximated as an infinitesimal dipole with a center frequency of 100 MHz. In each of the three crosshole data sets, 197 transmitter and 197 receiver locations were spaced equally at 0.075 m intervals between 1.95 and 16.65 m depth. After the FDTD modeling, the traveltimes of the direct transmitted wavefield were determined using a semiautomated picking procedure and then tomographically inverted for the subsurface electromagnetic velocity distribution using a nonlinear inversion scheme based on a finite-difference solution of the eikonal equation [*Lanz et al.*, 1998] with a inversion cell length of 0.3 m. Note that noise was not added to either the simulated GPR traces or picked travel times prior to the tomographic inversion for this study. Although not representative of realistic conditions, the addition of noise was deemed unnecessary for this work as its effect is to simply decrease data quality such that more regularization is required in the inversion procedure. This in turn results in a tomographic model with decreased resolution, which is addressed in the SA procedure by enforcing greater reliance on the target variogram function through the cutoff lag parameter.

[20] Figures 1d–1f show the velocity tomograms obtained from the inversion of the crosshole GPR traveltime data. A comparison of these images with the original porosity fields in Figures 1a–1c demonstrates that the velocity tomograms outline very well the larger-scale subsurface structures, but that structures smaller than the dominant GPR wavelength of approximately 1 m are not resolved. This smoothing is typical and results from the band-limited nature of the radar signal, the regularization applied in the tomographic inversion, and the fact that only traveltimes were used for the tomographic reconstruction. It clearly demonstrates why we require additional information at smaller scales to generate realistic porosity realizations.

3.3. Porosity Reconstruction Methods

[21] To evaluate the potential hydrological benefits of using our SA-based data integration procedure for the three

examples, we compare its performance with other more elementary methods to reconstruct the porosity field given the borehole log and/or crosshole GPR data. In the following we briefly describe each of the methods used, which we denote by the codes I, SS, T, and SA.

[22] I: This refers to horizontal linear interpolation between the porosity logs. Clearly this is an extremely basic technique that does not take into account the available crosshole GPR data, nor does it utilize any spatial statistical model for the porosity distribution. Nevertheless, we feel it is important to evaluate under what scenarios a simple method like linear interpolation might provide results that are as ''hydrologically useful'' as those provided by more sophisticated approaches involving geophysical methods. Only one realization is obtained with this approach.

[23] SS: This refers to the use of sequential Gaussian simulation to obtain the porosity field, given only the porosity log measurements and a prior variogram model. Again, the geophysical data are not used, but we try here to reproduce the spatial variability in the porosity field as prescribed by the variogram model. As the sequential simulation methodology has been thoroughly explained in several reference books [e.g., *Deutsch*, 2002; *Deutsch and Journel*, 1998; *Goovaerts*, 1997; *Kelkar and Perez*, 2002], we refer the reader to these books for detailed information. We base our SS approach on simple kriging and use the 40 nearest neighboring sampled points to estimate the kriging mean and variance at the randomly selected unsampled location [*Kelkar and Perez*, 2002]. The porosity value at that location is then drawn from a Gaussian distribution having this mean and variance. To obtain the variogram model required for this approach, we fit the vertical experimental variogram function of the porosity logs and assume that the aspect ratio between the horizontal and vertical directions is known (Table 1). For Examples 1–3, we generated 10 random realizations with the SS method. Solute transport simulations were then run on each realization.

[24] T: This refers to the process of converting directly the crosshole GPR tomographic velocity image to porosity using the $E(\phi|v)$ relationship established from the collocated data at the borehole locations. For each example, the parameters describing this linear relationship are provided in Table 1. Clearly, this approach does not at all address the fact that a crosshole GPR tomogram is in fact a spatial average of the underlying ''true'' parameters as a result of the ill-conditioned nature of the inverse problem and the regularization required to stabilize the solution [e.g., *Day-Lewis and Lane*, 2004]. Thus the resulting porosity field will lack the small-scale variability of the true model. However, it has not been thoroughly investigated whether such ''smoothed'' images of subsurface structure may, in many cases, contain enough information for reliable hydrological predictions.

[25] SA: This refers to the simulated annealing conditional simulation approach described earlier. For each perturbation of the realization in the SA process, we draw the new value from a Gaussian distribution having conditional expectation and variance defined in Table 1. This is done everywhere except at the borehole locations where we set the distribution to have a conditional expectation equal to the porosity log data and a small standard deviation of σ = 0.005. As mentioned, we obtain the vertical geostatistical model using the best fit to the experimental variogram function of the porosity logs at short lags. For the horizontal model, we assume that the aspect ratio between the horizontal and vertical directions is known. The cutoff lags, below which we constrain the output realizations to the variogram model, were set to 2 and 5 m in the vertical and horizontal directions, respectively. For Examples 1–3, 10 random realizations were again generated with this technique and tested with regard to their hydrological performance.

3.4. Groundwater Flow and Contaminant Transport Simulations

[26] After obtaining the hydraulic conductivity distribution from each porosity reconstruction using the relationship described in section 3.1, groundwater flow and solute transport simulations were performed. To do this, we assume an unconfined aquifer model with an impermeable boundary at the bottom and fixed head boundaries on either side. The hydraulic head at the inflow and outflow boundaries was set to 16.775 m and 16.475 m, respectively, which yielded an average hydraulic gradient equal to 0.01. For the tracer experiment, we set a constant concentration of 10 kg/m^3 of nonreactive solute along the left edge of the model from t = 0 onwards. The longitudinal and transverse dispersivities were specified to be 0.05 m, which is significantly smaller than the model cell size and thus implies that dispersion is largely governed by the underlying heterogeneity of our models.

[27] To simulate two-dimensional flow and transport, we used Comsol Multiphysics, a finite element analysis and solver program. First we solve for the steady-state spatial distribution of hydraulic heads on the basis of the Darcy flow equations. We then use this information to solve the transient advection-dispersion equations describing solute transport [e.g., *Freeze and Cherry*, 1979; *Pinder and Celia*, 2006; *Todd and Mays*, 2005]. Measurements of the tracer concentration are then assumed to be available all along the borehole on the right-hand side of the model, which provides us with ''breakthrough images'' of the concentration along this borehole in time and depth.

4. Results

[28] For each of the three example cases shown in Figures 1a–1c, we show in the left-hand column of Figures 2, 3, and 4 an example of one of the porosity fields obtained using each of the reconstruction techniques: I, SS, T, and SA. The true realization is shown again at the top and denoted by O. For each of the reconstruction methods the breakthrough image, showing the predicted solute concentration in the right-hand borehole as a function of depth and time, is shown in the middle column. In the right-hand column, we plot the absolute difference between the true breakthrough image and the one obtained from the reconstructions, with the mean absolute difference (MAD) value shown to the right of the plot as a general indicator of the quality of the prediction. Note that for both the SS and SA approaches, we chose for the sake of clarity to show only one realization out of a population of ten. For this we selected the realization that provides the fifth best hydrological prediction in terms of minimizing the MAD between the predicted and true breakthrough images. In other words, we take the median of ten realizations when considering the

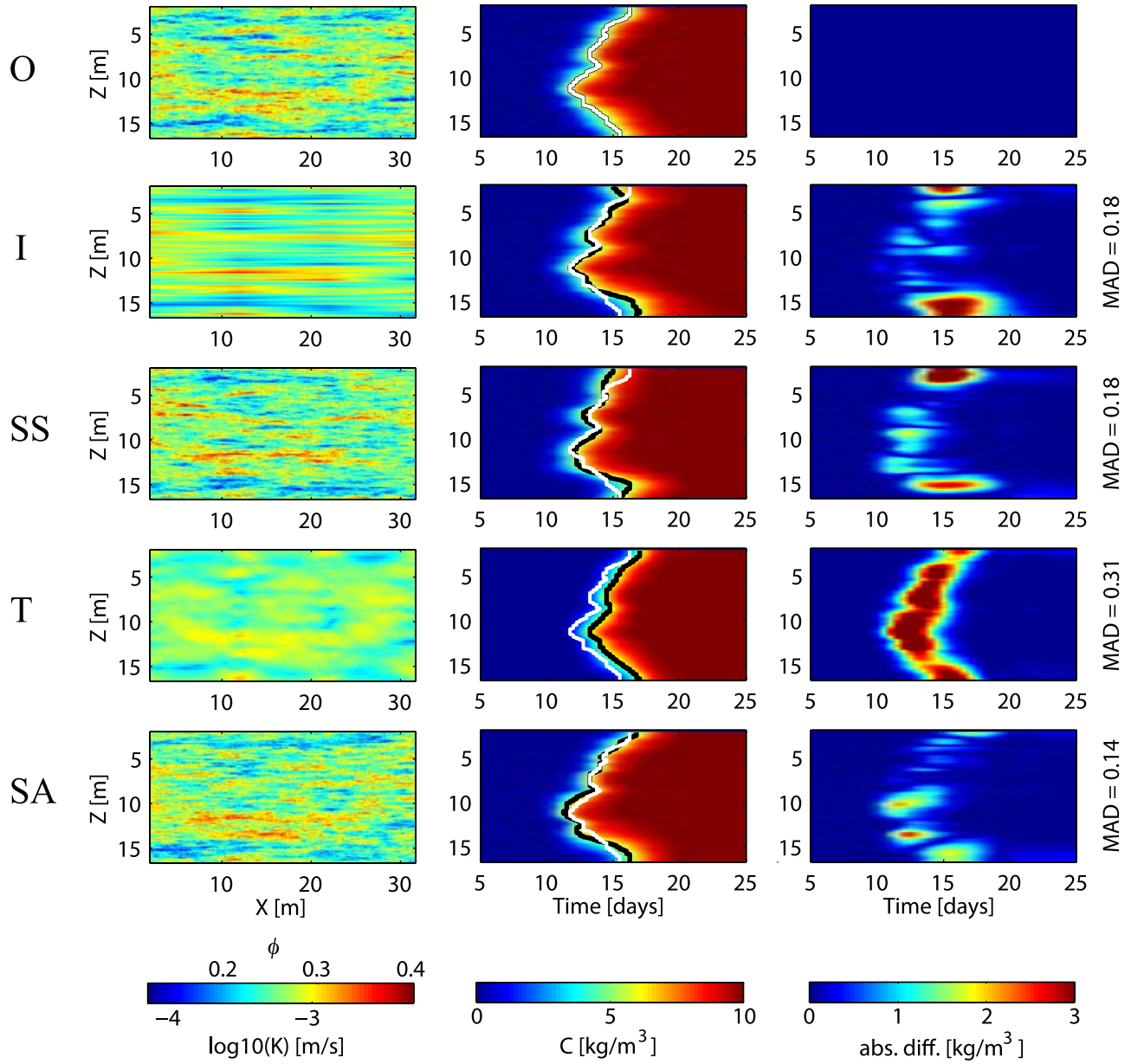

Figure 2. (left) Original ϕ/K distribution (O) and reconstructed ϕ/K fields obtained using the I, T, SS, and SA approaches for Example 1. (center) Corresponding breakthrough images, showing concentration in the right borehole as a function of time and depth. The white and black lines represent the time at which half of the maximum concentration is reached for the true and reconstructed fields, respectively. (right) Absolute difference between the true and reconstructed breakthrough images. The mean absolute difference (MAD) is shown to the right as a general indicator of goodness of fit.

hydrological performance compared to the true model. Although we admit that the use of 10 realizations is not enough to capture the true prediction uncertainty associated with the SS and SA techniques, we have found that it was more than sufficient in this study to provide an initial assessment of the hydrological benefits that these methods can bring.

4.1. Visual Comparison of the Reconstructed Porosity Fields

[29] For all three examples considered in Figures 2, 3 and 4, the comparison of the porosity fields obtained by linearly interpolating between the borehole logs (I) and the true porosity models (O) shows that, as expected, linear interpolation can only provide an acceptable approximation of the true porosity field if the horizontal correlation length is larger than the spacing between the boreholes (Figure 2). In this case, the borehole logs provide significant information about porosity in the interborehole region, and additional geophysical and geostatistical information is of limited benefit. Otherwise, linear interpolation provides simply a horizontally smoothed version of the true subsurface heterogeneity, which as we will see in the next section is not suitable for reliable flow and transport predictions.

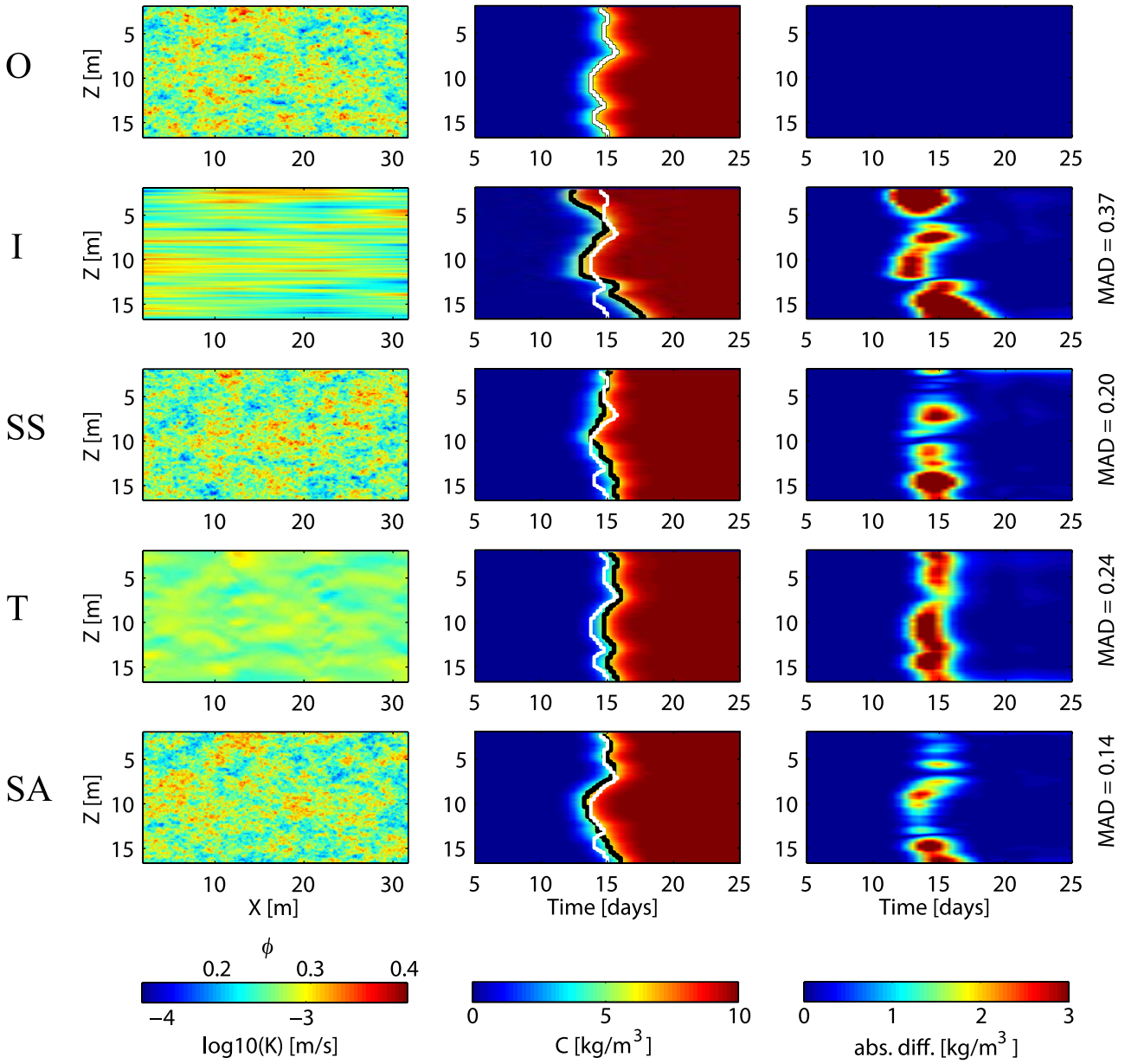

Figure 3. (left) Original ϕ/K distribution (O) and reconstructed ϕ/K fields obtained using the I, T, SS, and SA approaches for Example 2. (center) Corresponding breakthrough images, showing concentration in the right borehole as a function of time and depth. The white and black lines represent the time at which half of the maximum concentration is reached for the true and reconstructed fields, respectively. (right) Absolute difference between the true and reconstructed breakthrough images. The mean absolute difference (MAD) is shown to the right as a general indicator of goodness of fit.

[30] In the sequential simulation SS case, the porosity fields are reconstructed using both the borehole porosity logs and prior geostatistical information provided by the parametric target variogram function. Here we see that, for all three examples, the reconstructed porosity fields compare quite well with the original models in terms of the visible statistical nature of the heterogeneity. However, when the deterministic reproduction of the original porosity field is considered, only Example 1 shows a result that can be considered to be close to the truth (Figure 2). This again results from the large lateral correlation length used in Example 1, which allows the borehole porosity log data to provide the majority of information required for an accurate reconstruction. In Examples 2 and 3, much greater differences are present between the SS reconstructed and true fields because of the smaller lateral correlation lengths (Figures 3 and 4).

[31] In the case of the porosity reconstructions obtained by converting directly the tomographic GPR velocity image into porosity (T), we see a different behavior with changing aspect ratio and correlation length in the true model. Here, the T approach provides an acceptable reconstruction of the porosity field only for Example 3, which is described by a small aspect ratio and large vertical correlation length (Figure 4). This results because, in Example 3, the length scale of heterogeneity is larger than the dominant GPR

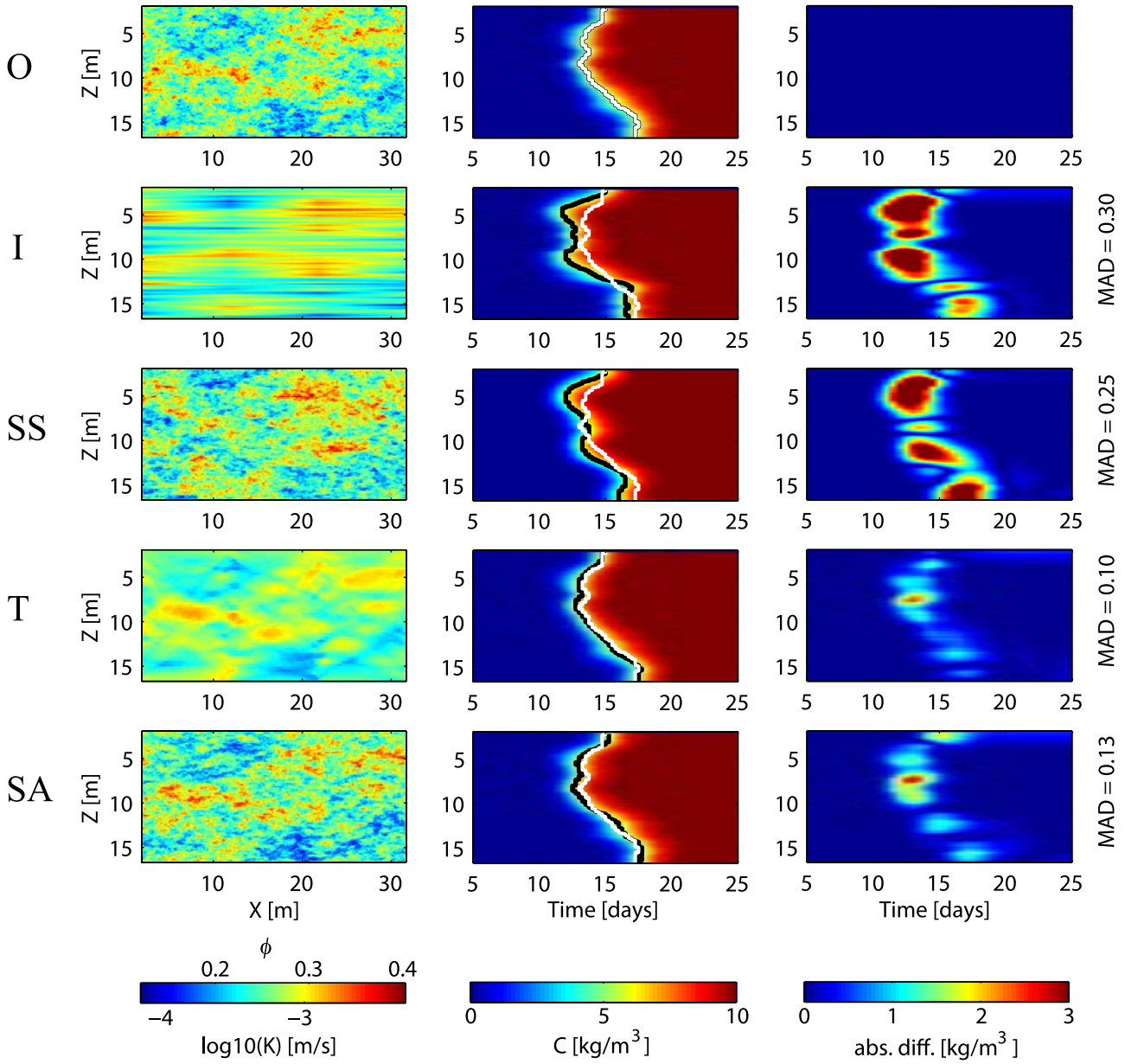

Figure 4. (left) Original ϕ/K distribution (O) and reconstructed ϕ/K fields obtained using the I, T, SS, and SA approaches for Example 3. (center) Corresponding breakthrough images, showing concentration in the right borehole as a function of time and depth. The white and black lines represent the time at which half of the maximum concentration is reached for the true and reconstructed fields, respectively. (right) Absolute difference between the true and reconstructed breakthrough images. The mean absolute difference (MAD) is shown to the right as a general indicator of goodness of fit.

wavelength, which means that the subsurface structural variability can be adequately imaged. Nevertheless, the T reconstruction in Example 3 is still a significantly smoothed version of the true porosity field, and thus lacks small-scale structures that may affect flow and transport. This only becomes worse in Examples 1 and 2, where the correlation lengths are smaller and thus the small-scale variability more significant.

[32] Finally we examine the SA method, which utilizes all available porosity log and crosshole GPR data for the reconstructions. Small-scale model structure with this method is provided by the parametric target variogram function, larger-scale structure by the GPR data, and the shape of the overall porosity histogram by the borehole log data and its relation to the GPR velocities. For all three examples, we see in Figures 2, 3 and 4 that the SA reconstructions agree most favorably with the original porosity models when compared to the other methods considered. Note especially that SA provides the most significant improvements compared to I and SS when the lateral continuity in the model is smaller than the distance between the boreholes (Figures 3 and 4). These results confirm that the SA-based approach is able to give reliable results independent of the structural variability. It should also be noted that, because the tomographic data are utilized in the SA procedure, the variability between the obtained

realizations is less than with the SS approach. This difference in variability between the SA and SS approaches can be seen to decrease as the horizontal correlation length increases, as in that case the porosity log data provide a significant amount of information about the interborehole porosity distribution.

4.2. Evaluation of Hydrological Behavior

[33] Looking at Figures 2, 3 and 4, it is clear, and after all not surprising, that differences in the spatial structure of the obtained porosity/hydraulic conductivity realizations have a significant impact on the solute transport predicted through these models. For simple linear interpolation between the borehole porosity logs (I), we see that the true hydrological behavior can only be well predicted in the case where the horizontal correlation length is larger than the borehole spacing. This is the case for Example 1, where we have an acceptable transport prediction with a MAD between the true and predicted breakthrough images equal to 0.18. For Examples 2 and 3, the obtained transport predictions are much worse, having MAD values of 0.37 and 0.30, respectively.

[34] With the SS method, we similarly see that the longer correlation length case of Example 1 yields the most accurate hydrological predictions. In this example, the predicted breakthrough images from the ten SS reconstructions had MAD values between 0.15 and 0.23, with the median value shown in Figure 2 equal to 0.18. In contrast, for Example 2, where we had much greater interborehole variablility between the ten realizations because of a shorter horizontal correlation length, the MAD values ranged between 0.17 and 0.29 with the median value equal to 0.20. For Example 3, we saw MAD values between 0.21 and 0.51 with the median value equal to 0.25. In this last case, the predicted breakthrough image very poorly estimates the true transport behavior even for the realization with the lowest MAD value. The main reason for this is that the mean of the borehole porosity data is not at all representative of the global mean of the true porosity field. Note that even using ordinary kriging and other parameters in the SS approach does not significantly change these findings.

[35] Contrary to the SS approach, the T approach shows a very good capacity to estimate the hydrological behavior for Example 3, providing the best prediction compared to the other methods with a MAD equal to 0.10. However, it is only in Example 3 where the tomographic reconstruction gives an acceptable transport prediction. This again results because the scale of heterogeneity in this case is larger than the dominant GPR wavelength, and thus the subsurface structural variability can be adequately imaged by the radar experiment. In Figures 2 and 3, for example, the MAD values of 0.31 and 0.24 are significantly larger. Nevertheless, significant similarities between the true and predicted breakthrough images can be seen with regards to the variability along the depth axis in Figures 2 and 3. That is, there is a more-or-less constant time shift between the true and predicted images, which is best seen from the white and black lines representing the time at which half the maximum tracer concentration is reached for the true and predicted fields, respectively. The reason for this shift is the underestimated variance of porosity with the T method, which when linked with a nonlinear relationship to the hydraulic conductivity strongly influences its mean and thus the average solute travel time. Therefore the result of the tracer experiment would clearly not be improved by varying the lateral and transverse dispersivity parameters compared to the potential use of a modified petrophysical relationship, calibrated to hydrological data. This is a topic that we are currently investigating.

[36] Finally, we consider the transport predictions obtained using the SA reconstruction method. Generally, by integrating both the borehole and tomographic data with this technique along with small-scale information from the supplied variogram model, we obtain the most accurate hydrological predictions. In Example 1, the MAD values between the true and predicted breakthrough images for the ten realizations created were between 0.12 and 0.18, with a median equal to 0.14 (Figure 2). In this case, because of the high lateral continuity between the boreholes, the improvements brought by the SA approach over the SS method are limited. Where the lateral correlation length is smaller than the distance between the boreholes, however, the SA method performs much better than SS, showing MAD values between 0.09 and 0.19 in Example 2, with a median equal to 0.14 (Figure 3), and between 0.11 and 0.16 in Example 3, with a median equal to 0.13 (Figure 4). From Example 2 it is clear that, when we are dealing with relatively small correlation lengths and with a scale of heterogeneity smaller than the dominant GPR wavelength, very good hydrological predictions can be obtained by incorporating tomographic geophysical data through conditional stochastic simulations. Further, when the scale of the heterogeneity is larger than the dominant GPR wavelength, such as in Example 3, we see that the SA approach does not always allow for improved hydrological predictions compared to the T approach. Clearly, the SA method shows the most benefit when compared to the other methods when the hydrological problem requires information at several scales because of its complexity.

5. Discussion and Conclusions

[37] The primary objective of this study was to investigate the potential hydrological benefits of incorporating high-resolution geophysical data into the subsurface characterization problem through a recently introduced SA conditional stochastic simulation method. We did this by evaluating hydrologically this method alongside other characterization approaches that utilize different amounts and types of subsurface information, again under optimal conditions. This was done for three hydrological property models, each having different heterogeneity characteristics, and within the context of assimilating borehole porosity log and crosshole GPR data to reconstruct the subsurface porosity field. On the basis of the assumption that there exists a unique and known grid-cell-scale relationship between porosity and hydraulic conductivity, we investigated whether the SA approach can offer significant hydrological benefits over the other methods, and if so, under what hydrological/structural circumstances these benefits are likely to be most significant.

[38] Visually, we saw that the porosity fields obtained by integrating crosshole GPR and borehole porosity log data using the SA-based approach had a significant degree of realism under all structural conditions studied. We can

therefore conclude that, with this method, detailed and seemingly realistic subsurface porosity distributions can be obtained independent of the heterogeneity characteristics, assuming of course that the utilized sources of data are of reliable quality. More importantly for this study, our hydrological evaluation of the estimated porosity distributions showed that the SA-based approach, in general, has the potential to yield much more reliable hydrological predictions than the other more elementary techniques. In particular, we found that SA provided the most significant improvements compared to I and SS when the lateral continuity in the model was smaller than the distance between the boreholes, and/or when the hydrological problem requires information at several scales because of its complexity. One notable exception occurred when the correlation length of the heterogeneity was greater than the dominant GPR wavelength. In this case, it seems that accurate hydrological predictions may also be made using the T approach, as the subsurface structural variability can be adequately imaged without the need for conditional simulations. It is important to note that the overall approach pursued in this study, as well as these key results, are expected to remain valid for all pertinent combinations of geophysical and borehole log data of comparable resolution and sensitivity to the hydrological target parameter, such as, for example, crosshole seismic and flowmeter log data.

[39] The above observations are clearly important to our understanding of how we can optimize the use of high-resolution geophysical data in hydrological studies. They allow us a much better understanding of when the use of an evolved data integration approach, such as the SA method, might potentially yield significant hydrological benefits and is worthwhile pursuing. However, for field applications, a number of important issues need to be further considered. First is the fact that, in reality, we are dealing with three-dimensional environments rather than the 2-D profiles considered here. Consequently, the results shown here are only valid for cases where heterogeneity in the third dimension is insignificant. Although the methods employed can still be expected to be valid for 3-D characterization, this will require adequate spatial coverage, resolution, and sensitivity of the geophysical data to the hydrologically pertinent parameters.

[40] Another critically important issue is that a large number of uncertainties and errors, which were purposely not considered in our evaluation, are present in real situations. This means that, in practice, each data set will need to be carefully considered in regard of its quality and reliability, and errors must be properly dealt with in the corresponding inversion and data integration procedures. Whereas errors in the borehole log measurements will influence all of the investigated approaches, errors in the geophysical data will have an impact on the T and SA approaches only. Clearly, errors in the geophysical data will be more adequately handled by the SA approach than the T approach because our use of a conditional distribution inferred from the collocated velocity and porosity measurements is sensitive to data quality. That is, the estimated conditional distribution will tend to be broader when the data are of lesser quality, which will result in greater uncertainty in the suite of output SA realizations. Note again that, because the velocity resolution with crosshole georadar tomography is worst at the borehole locations, the SA realizations will tend to be under- rather than overconstrained by the tomographic image. Further, the use of a cutoff lag with the SA method allows us to choose for what spatial scales we wish to rely on the tomographic image, taking into account its estimated resolution.

[41] Finally and most importantly, the largest limitation in applying the above approaches in the field comes from the uncertainty in the small-scale relationship between porosity and hydraulic conductivity. Clearly, we have assumed here the ideal case of being in a single hydrological unit where the relationship between these parameters is unique and known. Although this allowed us to investigate a number of important issues related to data integration using different approaches, the estimation of the distribution of hydraulic conductivity in the field will clearly need to make use of field-derived hydrological data to be most accurate. Evidently one important goal that we would like to achieve is to use reconstructions of geophysically derived property fields, such as the porosity fields obtained in this study, along with complementary information such as tracer test concentration data, to delineate various hydrological units and study possible relationships between the geophysical and hydrological parameters at the field scale. This is a topic of future research.

[42] **Acknowledgments.** This research was supported by a grant from the Swiss National Science Foundation. We also thank associate editor Fred Day-Lewis and the three anonymous referees whose comments helped to significantly improve this manuscript.

References

Asprion, U., and T. Aigner (1999), Towards realistic aquifer models: Three-dimensional georadar surveys of Quaternary gravel deltas (Singen Basin SW Germany), *Sediment. Geol.*, *129*(3–4), 281–297.

Beres, M., A. Green, P. Huggenberger, and H. Horstmeyer (1995), Mapping the architecture of glaciofluvial sediments with 3-dimensional georadar, *Geology*, *23*(12), 1087–1090.

Bowling, J. C., A. B. Rodriguez, D. L. Harry, and C. Zheng (2005), Delineating alluvial aquifer heterogeneity using resistivity and GPR data, *Ground Water*, *43*(6), 890–903.

Chen, J. S., S. Hubbard, and Y. Rubin (2001), Estimating the hydraulic conductivity at the South Oyster Site from geophysical tomographic data using Bayesian techniques based on the normal linear regression model, *Water Resour. Res.*, *37*(6), 1603–1613.

Dafflon, B., J. Irving, and K. Holliger (2009), Simulated-annealing-based conditional simulation for the local-scale characterization of heterogeneous aquifers, *J. Appl. Geophys.*, *68*(1), 60–70.

Davis, J. L., and A. P. Annan (1989), Ground-penetrating radar for high-resolution mapping of soil and rock stratigraphy, *Geophys. Prospect.*, *37*(5), 531–551.

Day-Lewis, F. D., and J. W. Lane (2004), Assessing the resolution-dependent utility of tomograms for geostatistics, *Geophys. Res. Lett.*, *31*(7), L07503, doi:10.1029/2004GL019617.

Day-Lewis, F. D., P. A. Hsieh, and S. M. Gorelick (2000), Identifying fracture-zone geometry using simulated annealing and hydraulic-connection data, *Water Resour. Res.*, *36*(7), 1707–1721.

Deutsch, C. V. (2002), *Geostatistical Reservoir Modeling*, 384 pp., Oxford Univ. Press, New York.

Deutsch, C. V., and A. G. Journel (1998), *GSLIB: Geostatistical Software Library and User's Guide*, 384 pp., Oxford Univ. Press, New York.

Deutsch, C. V., and P. W. Cockerham (1994), Practical considerations in the application of simulated annealing to stochastic simulation, *Math. Geol.*, *26*(1), 67–82.

Deutsch, C. V., and X. H. Wen (1998), An improved perturbation mechanism for simulated annealing simulation, *Math. Geol.*, *30*(7), 801–816.

Freeze, A. R., and J. A. Cherry (1979), *Groundwater*, 604 pp., Prentice-Hall, Englewood Cliffs, N. J.

Gelhar, L. W. (1993), *Stochastic Subsurface Hydrology*, 480 pp., Prentice-Hall, Englewood Cliffs, N. J.

Goovaerts, P. (1997), *Geostatistics for Natural Resources Evaluation*, 496 pp., Oxford Univ. Press, New York.

Harp, D. R., Z. X. Dai, A. V. Wolfsberg, J. A. Vrugt, B. A. Robinson, and V. V. Vesselinov (2008), Aquifer structure identification using stochastic inversion, *Geophys. Res. Lett.*, *35*(8), L08404, doi:10.1029/2008GL033585.

Heinz, J., S. Kleineidam, G. Teutsch, and T. Aigner (2003), Heterogeneity patterns of Quaternary glaciofluvial gravel bodies (SW-Germany): Application to hydrogeology, *Sediment. Geol.*, *158*(1–2), 1–23.

Holliger, K., and T. Bergmann (2002), Numerical modeling of borehole georadar data, *Geophysics*, *67*(4), 1249–1257.

Hubbard, S. S., and Y. Rubin (2005), Introduction to hydrogeophysics, in *Hydrogeophysics*, edited by Y. Rubin and S. S. Hubbard, pp. 3–21, Springer, Dordrecht, Netherlands.

Hubbard, S. S., Y. Rubin, and E. Majer (1999), Spatial correlation structure estimation using geophysical and hydrogeological data, *Water Resour. Res.*, *35*(6), 1809–1825.

Hubbard, S. S., J. S. Chen, J. Peterson, E. L. Majer, K. H. Williams, D. J. Swift, B. Mailloux, and Y. Rubin (2001), Hydrogeological characterization of the South Oyster Bacterial Transport Site using geophysical data, *Water Resour. Res.*, *37*(10), 2431–2456.

Hyndman, D. W., and S. M. Gorelick (1996), Estimating lithologic and transport properties in three dimensions using seismic and tracer data: The Kesterson aquifer, *Water Resour. Res.*, *32*(9), 2659–2670.

Hyndman, D. W., J. M. Harris, and S. M. Gorelick (2000), Inferring the relation between seismic slowness and hydraulic conductivity in heterogeneous aquifers, *Water Resour. Res.*, *36*(8), 2121–2132.

Kelkar, M., and G. Perez (2002), *Applied Geostatistics for Reservoir Characterization*, 264 pp., Soc. of Pet. Eng., Richardson, Tex.

Kowalsky, M. B., S. Finsterle, J. Peterson, S. Hubbard, Y. Rubin, E. Majer, A. Ward, and G. Gee (2005), Estimation of field-scale soil hydraulic and dielectric parameters through joint inversion of GPR and hydrological data, *Water Resour. Res.*, *41*(11), W11425, doi:10.1029/2005WR004237.

Lanz, E., H. Maurer, and A. G. Green (1998), Refraction tomography over a buried waste disposal site, *Geophysics*, *63*(4), 1414–1433.

Linde, N., S. Finsterle, and S. Hubbard (2006), Inversion of tracer test data using tomographic constraints, *Water Resour. Res.*, *42*(4), W04410, doi:10.1029/2004WR003806.

McKenna, S. A., and E. P. Poeter (1995), Field example of data fusion in site characterization, *Water Resour. Res.*, *31*(12), 3229–3240.

Paasche, H., J. Tronicke, K. Holliger, A. G. Green, and H. Maurer (2006), Integration of diverse physical-property models: Subsurface zonation and petrophysical parameter estimation based on fuzzy c-means cluster analyses, *Geophysics*, *71*(3), H33–H44.

Parks, K. P., L. R. Bentley, and A. S. Crowe (2000), Capturing geological realism in stochastic simulations of rock systems with Markov statistics and simulated annealing, *J. Sediment. Res.*, *70*(4), 803–813.

Pinder, G. F., and M. A. Celia (2006), *Subsurface Hydrology*, 488 pp., John Wiley, Hoboken, N. J.

Robinson, D. A., et al. (2008), Advancing process-based watershed hydrological research using near-surface geophysics: A vision for, and review of, electrical and magnetic geophysical methods, *Hydrol. Processes*, *22*(18), 3604–3635.

Scheibe, T. D., and Y. J. Chien (2003), An evaluation of conditioning data for solute transport prediction, *Ground Water*, *41*(2), 128–141.

Schön, J. H. (2004), *Physical Properties of Rocks: Fundamentals and Principles of Petrophysics*, 583 pp., Elsevier, Oxford, U. K.

Sudicky, E. A., and P. S. Huyakorn (1991), Contaminant migration in imperfectly known heterogeneous groundwater systems, *Rev. Geophys.*, *29*(S), 240–253.

Todd, D. K., and L. W. Mays (2005), *Groundwater Hydrology*, 656 pp., John Wiley, Hoboken, N. J.

Tronicke, J., and K. Holliger (2005), Quantitative integration of hydrogeophysical data: Conditional geostatistical simulation for characterizing heterogeneous alluvial aquifers, *Geophysics*, *70*(3), H1–H10.

Zheng, C. M., and S. M. Gorelick (2003), Analysis of solute transport in flow fields influenced by preferential flowpaths at the decimeter scale, *Ground Water*, *41*(2), 142–155.

B. Dafflon, K. Holliger, and J. Irving, Institute of Geophysics, Faculty of Geosciences and Environment, University of Lausanne, Amphipôle Building, CH-1015 Lausanne, Switzerland. (baptiste.dafflon@unil.ch; klaus.holliger@unil.ch)